

Received August 1, 2020, accepted September 2, 2020, date of publication September 9, 2020, date of current version September 25, 2020.

Digital Object Identifier 10.1109/ACCESS.2020.3023024

# Monitoring and Risk Assessment of Wildfires in the Corridors of High-Voltage Transmission Lines

YU LIANG<sup>1</sup>, LAWU ZHOU<sup>1</sup>, JIE CHEN<sup>2</sup>, YONG HUANG<sup>3</sup>, RUIZENG WEI<sup>3</sup>, AND ENZE ZHOU<sup>3</sup>

<sup>1</sup>School of Electrical and Information Engineering, Changsha University of Science and Technology, Changsha 410114, China

<sup>2</sup>National Satellite Meteorological Center, Beijing 100081, China

<sup>3</sup>Electric Power Research Institute of Guangdong Power Grid Company Ltd., Guangzhou 510080, China

Corresponding authors: Lawu Zhou (zhoulawu@csust.edu.cn) and Jie Chen (chenjie@cma.gov.cn)

This work was supported in part by the National Natural Science Foundation of China under Grant 41775162, and in part by the Electric Power Research Institute, Guangdong Power Grid Company Ltd., under Grant GDKJXM20173024.

**ABSTRACT** The scale of China's power grid is becoming larger and larger, more and more high-voltage long-distance overhead transmission lines are exposed to the wild environment. Wildfire disasters seriously threaten the safety and stability of transmission lines. In order to monitor and warn the fire points that may affect the operation of the transmission line in advance, this research is carried out. Suomi National Polar-orbiting Partnership (Suomi NPP) polar orbiting satellite and Himawari-8 geostationary satellite are used to monitor wildfires in a complementary manner, combined with improved relative threshold and adaptive dynamic threshold to identify fire points based on background radiation information. Then, a fire risk assessment system based on the entropy weight method and variable weight theory for transmission line corridors was constructed from four aspects: meteorology, underlying surface, topography and power grid. Engineering practice shows that the method proposed in this study effectively monitors and scientifically warns wildfires in the transmission line corridor, which greatly reduces the losses and working pressure caused by wildfires.


**INDEX TERMS** Suomi NPP polar orbiting satellite, Himawari-8 geostationary satellite, improved relative threshold, adaptive dynamic threshold, entropy weight method, variable weight theory.

## I. INTRODUCTION

The imbalance of China's energy distribution pattern and economic development level requires the use of long-distance transmission lines to transfer electrical energy from the power generation center to the load center. Many lines pass through densely vegetated forests and mountains, and wildfires caused by human or lightning seriously threaten the insulation safety and operation reliability of transmission lines [1]. High-voltage transmission lines are usually set up in double or multiple circuits on the same tower. Wildfires may cause multiple circuits to trip simultaneously or successively, and reclosing is often difficult to succeed. Manual power transmission can only be carried out after the thick smoke dissipates, so the line shutdown time caused by wildfires is generally longer [2]. Historical data shows that the forced shutdown faults caused by wildfire accounted for 79% and 64% of the total faults in the 220kV and 500kV line forced shutdowns for more than 30 minutes [3]. The formation of

wildfires is greatly affected by industrial and agricultural production. The tripling-faults of transmission lines caused by wildfires are mainly concentrated in the periods of Spring Festival, Tomb-sweeping Festival, spring ploughing, autumn harvest and extreme drought. Meanwhile, most of them are concentrated at 12:00~17:00 under the influence of strong winds and other factors, showing a high concentration in a short time [4]. Under the influence of wildfires in the spring of 2014, there were 47 emergency stop operations, 17 reduced-voltage operations, and 213 exit reclosing operations of the State Grid Corporation's 220 kV and above lines [5]. In the past five years from 2014 to 2018, wildfires near transmission line in five provinces under the jurisdiction of China Southern Power Grid co., Ltd. caused a total of 54 trips, and only 21 lines reclosed successfully accounted for less than 50%. Therefore, there is an urgent need for monitoring and warning of wildfires in the transmission line corridor to ensure safe and stable operation of the power grid.

The traditional method of monitoring wildfires near transmission lines is to combine observation towers with aircraft cruises. The obtained wildfire monitoring data is not accurate

The associate editor coordinating the review of this manuscript and approving it for publication was Zhiyi Li .

and the monitoring cost is high. The scope and frequency of observations are also very limited, and wildfires could not be found in time. In order to effectively monitor wildfires that may affect the operation of transmission lines, a variety of monitoring methods have emerged, including installation of pyrotechnic detection devices at fixed locations [6], meteorological radar monitoring [7], and meteorological satellite remote sensing. Meteorological satellite remote sensing is the most widely used macro monitoring technology for wildfire monitoring at home and abroad, with advantages of wide monitoring range, short monitoring cycle and high spatial resolution [8]. In order to accurately identify the fire point, scholars at home and abroad have carried out research on the fire point identification algorithm based on polar orbit satellite data, and proposed threshold method, context fire point identification method and three-band synthesis method [9]–[11], where threshold method can be divided into absolute threshold method and relative threshold method [12], [13]. The spatiotemporal context algorithm based on Himawari-8 geostationary satellite data was proposed by Xie [14], which was applied to fires in East Asia and Australia in 2016. The results show that the algorithm has higher monitoring accuracy than the traditional context and time algorithm. The above fire point identification method applied to the forestry department is only applicable to the monitoring of fire in large areas of forests, grasslands, straws, etc. However, for small-scale wildfires that can cause transmission line to trip, the traditional forestry department's identification method can no longer meet the needs of the power grid [15]. In order to monitor wildfires in the transmission line corridors, domestic scholars have carried out many studies. In order to improve the accuracy of low temperature fire point identification, a fire point identification algorithm for transmission lines based on probability statistics is proposed by Jiang and Yan [16]. In order to monitor small-scale fire in the transmission line corridor, a comprehensive threshold algorithm based on coarse judgment and fine judgment was proposed by Lu *et al.* [17]. The above methods have been applied to the provincial power grid system and have achieved good results. However, these methods all use single satellite data, which is easy to cause the phenomenon of wildfire leakage alarm. The fire point monitored by the satellite should be quickly judged whether it will affect the operation of the transmission line. The currently more practical risk assessment strategy for wildfires in the transmission line corridor is based on the distance between the fire point and the line, and the warning is graded by kilometers [15]. During the period of high incidence of wildfires, multiple fire points that affect the operation of transmission lines may be simultaneously detected in the same area. However, the probability of tripping on transmission lines caused by wildfires of different intensities is different, and the damage of tripping on transmission lines of different importance degrees to the power grid is also different. The evaluation is based on only a single element, which cannot propose an effective scientific basis for firefighting of transmission lines.

Polar orbiting satellites are limited by transit time, and there are only 2~4 opportunities a day to identify fire points in the same area. It is not possible to identify fire points outside the revisit time and cannot monitor 24 hours uninterruptedly. The resolution of geostationary satellites far from the surface is generally lower than that of polar-orbiting satellites, and there are a certain number of missing judgments for tiny fire points. This paper proposes a complementary monitoring method for wildfires in transmission line corridors based on the high-precision characteristics of Suomi NPP and the high-frequency characteristics of Himawari-8. Then, combined with the improved relative threshold condition and adaptive dynamic threshold, the fire point is identified based on the background radiation signal. Finally, a variety of elements are integrated to evaluate fire risk level and issue an alarm. At present, the system has been applied to the wildfire monitoring and warning center of China Southern Power Grid, which has enhanced the emergency response capacity of the power grid in the case of wildfire disaster and effectively reduced tripping accidents of transmission lines.

## II. COMPLEMENTARY MONITORING OF WILDFIRES BASED ON SATELLITE REMOTE SENSING

### A. INTRODUCTION TO METEOROLOGICAL SATELLITE

Polar orbit meteorological satellites are also called solar synchronous orbit meteorological satellites. Their orbit is 650 ~ 1500 km above the earth, and they run around the north and south poles of the earth with a period of about 115 minutes. The advantage is that they cover the whole world and have a wide field of observation. Geostationary meteorological satellites work in geosynchronous orbit around 35,800 km above the equator, they can observe a fixed area of one third of the earth's surface, and perform high-frequency meteorological observations on the target area. At present, the main satellite instruments and their characteristics commonly used for fire point identification in China are shown in Table 1. Although the time resolution of polar orbiting satellites is low, the spatial resolution is high. In the case of the same pixel area percentage  $P$ , the sensitivity of Suomi NPP is about 2 times higher than that of general polar orbit satellites and 7 times higher than that of geostationary satellites. Suomi NPP satellite has a strong ability to monitor small fire points, and its revisit time coincides with the time when wildfires occur frequently every day, which provides a stronger guarantee for the monitoring of wildfires in the transmission line corridor [17]. The positioning deviation of the satellite is also an issue that needs to be considered in the process of monitoring the fire point. The farthest positioning deviation of the pixel itself is the length of the half diagonal of the pixel [18]. Suomi NPP is about 3/4 of the general polar orbit satellites, about 3/8 of the geostationary satellites. Although the geostationary satellite differs greatly from the polar orbit satellite in terms of accuracy, it can monitor the target area 24 hours a day. Figure 1 shows the fire incident on the grassland outside Hulunbuir City, Inner Mongolia Autonomous Region, China

TABLE 1. Main satellite instruments for meteorological satellite remote sensing fire monitoring.

Satellite type	Satellite/Instrument	Resolution/m	Sensitivity/P	Positioning deviation/m	Revisit period/Observation frequency
Polar orbiting meteorological satellite	FY-3/VIRR	1000	1×1	1000√2/2	2 times/day
	EOS/MODIS	1000	1×1	1000√2/2	2 times/day
	NOAA/AVHRR	1000	1×1	1000√2/2	2 times/day
	Suomi NPP/VIIRS	750	0.75×0.75	750√2/2	2 times/day
Geostationary meteorological satellite	FY-4/AGRI	2000	2×2	2000√2/2	15 minutes/time
	Himawari-8/AHI	2000	2×2	2000√2/2	10 minutes/time

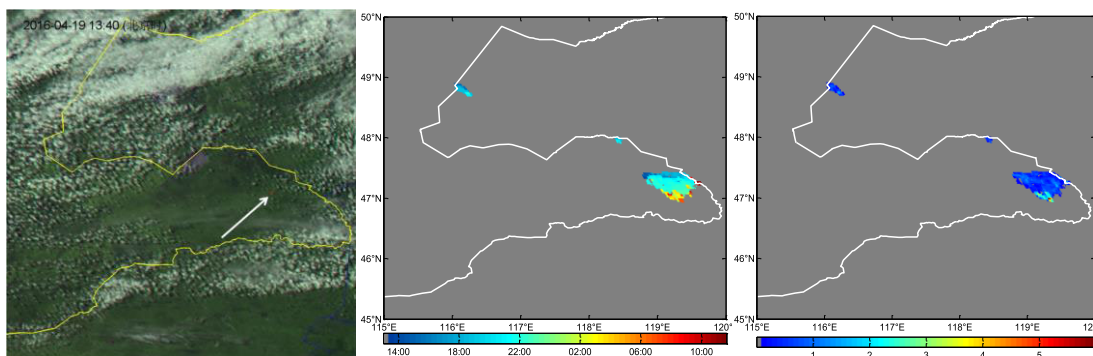


FIGURE 1. Fire point development process monitoring.

at 13:40 on April 19, 2016. Himawari-8 continuously monitored the dynamic development process of the fire at an interval of 10 minutes. This paper combines the characteristics of Suomi NPP and Himawari-8 to monitor wildfires in a complementary manner.

1) SUOMI NPP POLAR ORBITING METEOROLOGICAL SATELLITE

Suomi NPP was launched from Vandenberg Air Force Base, California, USA on October 28, 2011[19]. The Suomi NPP satellite operates in a descending orbit, it can orbit the earth about 14 times a day and observe the earth’s surface twice [20], [21]. The Suomi NPP satellite is equipped with five ground observation instruments for the JPSS mission. Visible Infrared Imaging Radiometer Suite (VIIRS) is the expansion and improvement of NOAA high-resolution radiometer AVHRR and NASA medium-resolution imaging spectrometer MODIS [22]. The VIIRS instrument is a whiskbroom scanning radiometer with a field of regard of 112.56° in the cross-track direction. It operates at a nominal height of 829 km from the ground, passes through the equator every 4 hours, and has a scanning width of 3060 km. VIIRS has a total of 22 spectral bands, including 16 medium resolution bands, 5 imaging resolution bands, and a panchromatic day and night band [23].

2) HIMAWARI-8 GEOSTATIONARY METEOROLOGICAL SATELLITE

Himawari-8 geostationary meteorological satellite was launched by the Japan Meteorological Agency from

Tanegashima Space Center on October 7, 2014 and officially began operation on July 7, 2015. The satellite is located at  $3.58 \times 10^4$  km above the equator at 140.7° east longitude and uses 3-axis attitude control technology [24]. The satellite can observe 6 observation points in five regions, including the whole disk, Japan area, target area and landmark area, and the observation period of the whole disk is 10 minutes [25]. The built-in Advanced Himawari Imager (AHI) contains a total of 16 bands from visible light to infrared light, of which the red light band has a spatial resolution of 500 m, the green light, blue light and 0.86 μm near infrared bands have a spatial resolution of 1 km, and the remaining 12 The spatial resolution of each band is 2 km [26]. The multi-band band setting and high temporal resolution feature of the satellite can realize 24-hour continuous monitoring of wildfire under cloudless conditions.

B. PROCESS OF FIRE POINT IDENTIFICATION

The preprocessing of satellite data is the basis of interference pixel detection and fire points identification. The satellite data is analyzed, corrected for radiation, corrected for positioning, enhanced synthesis processing and projection conversion to facilitate subsequent operations. The preprocessed satellite data is respectively used to identify water bodies, flares and cloud pixels, so as to reduce the influence of interfering pixels on fire points identification. Extract some suspicious fire point pixels, and then calculate the background brightness temperature of each suspicious fire point. If the background brightness temperature of the pixel is successfully calculated within a reasonably expanded background window area,

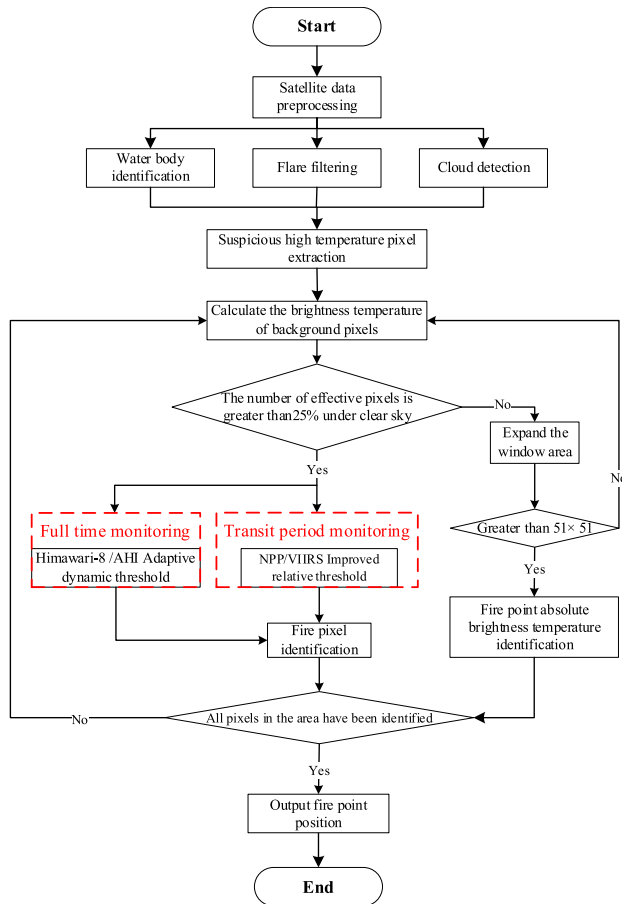


FIGURE 2. Flow chart of identification of wildfire near transmission line based on multi-source satellite.

Himawari-8 uses adaptive dynamic thresholds and Suomi NPP uses improved relative threshold for identification. If the conditions are met, it is the real fire point. Otherwise, it is a false fire point. If the background brightness temperature of the pixel is not successfully calculated within the reasonably expanded background window area, the absolute threshold condition is used for identification.

C. ELIMINATION OF DISTURBING PIXELS

1) IDENTIFICATION OF WATER BODIES

Based on the natural properties of water bodies, it is almost impossible to cause fire, and a flare phenomenon will occur when the water body forms a certain angle with the sun. so it is necessary to exclude the influence of the water pixels before the determination of the fire point. Using the global 30m resolution surface coverage data provided by GlobeLand30 [27] to draw the underlying surface types of some areas in southern China as shown in Figure 3, the lower right is a partial enlarged view of the Pearl River Delta, which can clearly identify the underlying surface type of the target area. Water bodies are determined by comparing the surface type of GlobeLand30 underlying surface in the area to be judged. If it is determined as a water pixel, fire point identification is not performed.

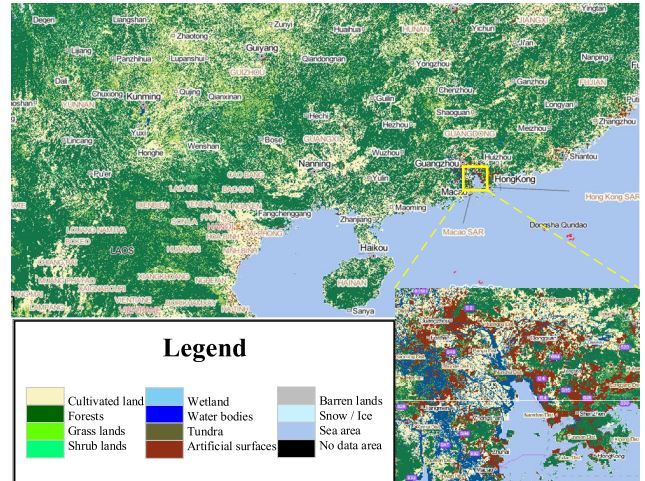


FIGURE 3. Distribution map of the underlying surface types in some areas of southern China.

2) IDENTIFICATION OF FLARES

Flare point refers to the phenomenon that the specular reflection of sunlight received by satellite sensors causes a sharp rise in radiant bright temperature under appropriate observation conditions. The presence of flare may cause misjudgment of ignition during the day, so the influence of flare should be filtered out before extracting the suspected fire point. The flare region does not show up in the infrared band data, but there is a large mutation in the visible light band data. Combining the infrared and visible light band data can better identify the solar flare region [28].

Calculation formula of flare angle  $\theta_r$  [29]:

$$\theta_r = \sin \theta_V \cdot \sin \theta_s \cdot \cos \psi + \cos \theta_V \cdot \cos \theta_s \quad (1)$$

where:  $\theta_V$  is the zenith angle of observation;  $\theta_s$  is the solar altitude angle;  $\psi$  is the relative azimuth angle. If the pixel satisfies the condition of formula (2), there is no need for fire identification in the flare area [30].

$$\begin{cases} R_{I1}, R_{I2}, R_3, R_4 > 0.3 \\ \theta_r < 40^\circ \end{cases} \quad (2)$$

where:  $R$  is the apparent reflectance of a certain band of VIIRS or AHI.

3) CLOUD DETECTION

Cloud, as the most common and uncertain underlying surface element, cannot be ignored for its influence on fire point identification [31]. In order to reduce the influence of cloud pixels on fire point identification, cloud detection is used to identify cloud pollution pixels. The most commonly used cloud detection algorithm is to use the spectral information or texture information of remote sensing images to distinguish clouds from ground objects [32]. Whether it is a single cloud detection algorithm or a combination of multiple algorithms, the multi-band threshold method will be applied. This method is also the cloud detection algorithm commonly used by all

domestic and foreign satellite data processing application departments. The only difference lies in the optimal combination of bands and the selection of threshold [28]. According to the requirements of Suomi NPP and Himawari-8 satellite data and optimized band, a multi-threshold condition algorithm suitable for most areas in southern China is proposed, as follows:

$$R_{I1} + R_{M7} > 0.9 \text{ or } R_3 + R_4 > 0.9 \quad (3)$$

$$T_{M16} < 265K \text{ or } T_{14} < 265K \quad (4)$$

$$\begin{cases} 0.7 < R_{I1} + R_{M7} \leq 0.9 \\ 265K \leq T_{M16} < 285K \end{cases} \text{ or } \begin{cases} 0.7 < R_3 + R_4 \leq 0.9 \\ 265K \leq T_{14} < 285K \end{cases} \quad (5)$$

where:  $T$  is the apparent brightness temperature of a certain band of VIIRS or AHI. In the daytime, pixels to be determined can be identified as cloud pixels if they meet any of the equations (3), (4) or (5). At night, the pixel to be judged as a cloud pixel only satisfies formula (4).

### D. FIRE POINT IDENTIFICATION MODEL

#### 1) IMPROVED RELATIVE THRESHOLD BASED ON VIIRS

For the pixels to be determined on cloudless land (excluding the influence of water bodies and flares, if equation (6) is satisfied in the daytime or equation (7) is satisfied at night, the pixels will be judged as suspicious fire pixels; otherwise, they will be non-fire pixels.

$$\begin{cases} T_{M13} > 310K \\ \Delta T_{13-15} > 10K \\ R_{I2} < 0.3 \end{cases} \quad (6)$$

$$\begin{cases} T_{M13} > 305K \\ \Delta T_{13-15} > 10K \end{cases} \quad (7)$$

where:  $\Delta T_{13-15}$  is the apparent brightness temperature difference between M13 and M15 bands of VIIRS.

The background bright temperature of the suspicious fire point is calculated on the basis of determining that the pixel is a suspicious fire point. A rectangular background window consisting of  $N \times N$  pixels was established with the suspected fire pixel as the center, in which the water pixel was denoted as  $N_W$ , the flare pixel as  $N_S$ , and the cloud pixel as  $N_C$ . The pixel satisfying the formula (8) or (9) in the day or night was denoted as  $N_F$ .

$$\begin{cases} T_{M13} > 325K \\ \Delta T_{13-15} > 20K \end{cases} \quad (8)$$

$$\begin{cases} T_{M13} > 310K \\ \Delta T_{13-15} > 10K \end{cases} \quad (9)$$

When the background light temperature is calculated, it is required that the neighborhood pixels in the window exclude  $N_W$ ,  $N_S$  and  $N_C$ . The remaining background pixels are valid

background pixels, denoting as  $N_E$ . In order to ensure sufficient radiation difference between the background window area and the suspected fire point, the window area initialized to  $3 \times 3$  grid points uses the split window algorithm to start the identification of each pixel, and all analysis points in the total pixel should have no less than 25% effective background pixels and  $N_E$  is greater than 8 [33]. If the above conditions are not met, the initial window area is expanded to  $5 \times 5$ ,  $7 \times 7$ , ...,  $49 \times 49$ ,  $51 \times 51$  as shown in Figure 4 until the condition is satisfied. The method can reduce the influence of different underlying surface types and mountain fire sizes on the calculation of background bright temperature, thus ensuring the accuracy of fire point extraction and the spatial applicability of the algorithm [34]. If there is not enough effective background pixel when  $N = 51$ , the absolute threshold condition is used for fire point identification. When the 10-band brightness temperature of VIIRS is greater than 360K during the day or greater than 320K at night, it can be directly determined that the pixel is a fire point pixel, otherwise, the identification of the pixel is abandoned.

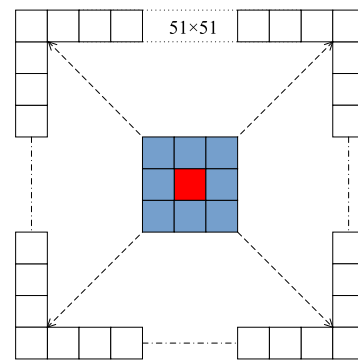


FIGURE 4. Background window area expansion.

Considering the diversified underlying surface types of various provinces and regions of China Southern Power Grid, and Suomi NPP sensitivity is higher than that of general polar orbit satellites. Under the condition of traditional relative threshold identification, the number of missed judgments is greatly reduced but the number of misjudgments is significantly increased. Conventional thermal anomalies on the underside of factory smokestacks, photovoltaic power stations and urban agglomerations can easily be mistaken for wildfires. To solve this problem, an improved relative threshold condition is proposed, and a brightness temperature difference correction coefficient  $\delta T^*$  is added. The analysis of thermal anomalies is shown in Figure 5. When the bright temperature difference is corrected to 5K, the fire spot identification accuracy is about 45%. When the bright temperature difference is corrected to 6K, the accuracy is close to 50%. When the bright temperature difference is corrected to 8K, the accuracy is close to 70%. When the bright temperature difference is corrected to 10K, the accuracy reaches 85%. When the bright temperature difference is corrected to 12K, the accuracy drops to 80%, and the temperature difference

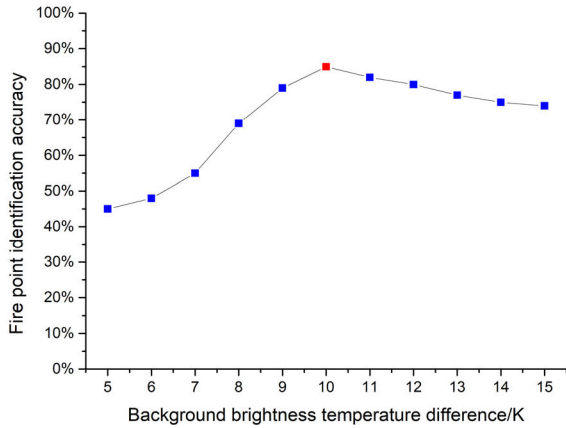


FIGURE 5. Relationship curve between identification accuracy and brightness temperature difference correction coefficient.

correction coefficient continues to increase and the accuracy gently declines.

Increasing the difference in background brightness temperature to 10K can significantly reduce the misjudgment of the fire point. When the window area contains a sufficient number of effective background pixels, it is compared with the brightness temperature characteristic of the suspicious fire point to obtain the improved relative threshold, as follows:

$$\Delta T_{13-15} > \overline{\Delta T_{E13-15}} + 3.5\delta\Delta T_{E13-15} + 4K \quad (10)$$

$$\Delta T_{13-15} > \overline{\Delta T_{E13-15}} + 10K \quad (11)$$

$$T_{M13} > \overline{T_{EM13}} + 3\delta\Delta T_{EM13} + 10K \quad (12)$$

$$T_{M15} > \overline{T_{EM15}} + \delta\Delta T_{EM15} - 4K \quad (13)$$

$$\delta T_{WFM13} > 5K \quad (14)$$

where:  $\overline{T_{EM13}}$  and  $\delta\Delta T_{EM13}$  are the mean and mean absolute deviations of M13 band bright temperature of the effective background pixel respectively;  $\overline{T_{EM15}}$  and  $\delta\Delta T_{EM15}$  are the mean and mean absolute deviations of M15 band bright temperature of the effective background pixel respectively;  $\overline{\Delta T_{E13-15}}$  and  $\delta\Delta T_{E13-15}$  are mean and mean absolute deviations of bright temperature difference of effective background pixel M13 and M15 bands respectively;  $\delta T_{WFM13}$  is the average absolute deviation of the background ignition point image M13 band bright temperature in the window [35]. If the formula (10, 11, 12, 13) or (10, 11, 12, 14) is true during the daytime, then the suspected fire spot is determined to be the real one; if the formula (10, 11, 12) is true at night, the suspected fire spot can be determined as the real one. Otherwise, it will be marked as a false one.

## 2) ADAPTIVE DYNAMIC THRESHOLD BASED ON AHI

The operational altitude and observation mode of geostationary meteorological satellites are different from those of polar orbiting satellites, so the traditional fire point identification algorithm based on polar orbiting satellites cannot be directly applied to geostationary meteorological satellites. The calculation of background bright temperature is the key to the

identification of fire pixels, which has a direct impact on the accuracy of identification. The initial size of the background window area is  $3 \times 3$  pixels, the bright temperature of the background pixel is the average temperature of the background pixel in the window area (except water body, flare, cloud and high temperature suspicious fire point pixel), as follows:

$$T_{ib} = \sum_{k=1}^n T_i/n \quad (15)$$

where:  $T_{ib}$  is the background brightness temperature value of the  $i$ -band of AHI;  $T_i$  is the brightness temperature of the  $i$ -band adjacent to the pixel to be judged;  $n$  is the number of adjacent pixels. The identification conditions of the suspicious fire point pixels determined by the years of experience of fire point identification of China National Satellite Meteorological Center are as follows:

$$T_7 > \overline{T_7} + 2\delta T_7 \quad (16)$$

$$T_7 > \overline{T'_{7b}} + 2.5\delta T'_{7b} \quad (17)$$

where:  $\overline{T'_{7b}}$  is the average brightness temperature of band 7 of the same pixel in the window area as the land use type of the pixel to be judged,  $\delta T'_{7b}$  is the standard deviation of the band 7 brightness temperature of the same pixel in the window area as the land use type of the pixel to be determined.

If the effective background pixels satisfying the above conditions in the  $3 \times 3$  window area are less than 25%, expand the window area to  $5 \times 5$ ,  $7 \times 7$ , ...,  $51 \times 51$  as shown in Figure 4. If the requirements are still not met, absolute threshold conditions are used for fire point identification. When the bright temperature of the AHI band 7 is greater than 360K in the daytime or 320K at night, the pixel can be directly identified as a fire point pixel; otherwise, the pixel is abandoned. When a sufficient number of valid background pixels are contained in the window area, adaptive dynamic threshold will be used for identification, as follows:

$$T_7 > T_{E7b} + n_1^*\delta T_{E7b} \quad (18)$$

$$T_{7-14} > T_{E7-14b} + n_2^*\delta T_{E7-14b} \quad (19)$$

where:  $\delta T_{E7b}$  represents the standard deviation of the 7-band brightness temperature of the background window area AHI;  $T_{E7-14b}$  represents the average value of the background window  $T_{7-14}$ ;  $\delta T_{E7-14b}$  represents the standard deviation of the background window  $T_{7-14}$ . The main purpose of setting this condition is to distinguish the difference in the inherent bright temperature values of the pixels of different underlying surface types in the window. When the proportion of the pixels in the window area is relatively consistent, the values of  $\delta T_{E7b}$  and  $\delta T_{E7-14b}$  are relatively small. In the process of fire point identification, when  $\delta T_{E7b}$  and  $\delta T_{E7-14b}$  are less than 2K, use 2K instead; when greater than 4K, use 4K instead. The National Satellite Meteorological Center analyzed the influence of the solar height angle  $\theta_s$  of the pixels to be identified and the proportion  $P$  of the non-vegetable pixels

in the window area on the background coefficient based on a large number of real historical fire points, as follows:

$$n_k^* = \begin{cases} n_k \cdot (1 + \sin \theta_s) \cdot (1 + P) & \theta_s \leq 45^\circ \\ n_k \cdot (1 + 1.2 \sin \theta_s) \cdot (1 + P) & \theta_s > 45^\circ \end{cases} \quad (20)$$

where:  $k = 1, 2$ ;  $n_1 = 3$ ;  $n_2 = 3.5$ ;  $n_k^*$  is the correction coefficient of the background, which changes with different areas, different times and different angles.

**E. FIRE POINT LOCATION BASED ON REFINED GRID**

The disk image captured by the satellite is projected onto the plane rectangular latitude and longitude coordinate system by means of calibration and positioning before the fire point identification. The difference in resolution between the two types of coordinate systems results in vacant pixels in the projected plane coordinate system, which is usually filled by interpolation. Interpolation calculations around the fire point cells will increase the number of fire pixels. In order to improve the accuracy of the fire point coordinates, the pixels with a lower brightness temperature value among all the adjacent fire pixels are eliminated before the output of the fire point coordinates. Combine the remaining fire pixels to obtain the entire fire zone, the center of the fire zone is used as the fire point coordinate output as shown in Figure 6.

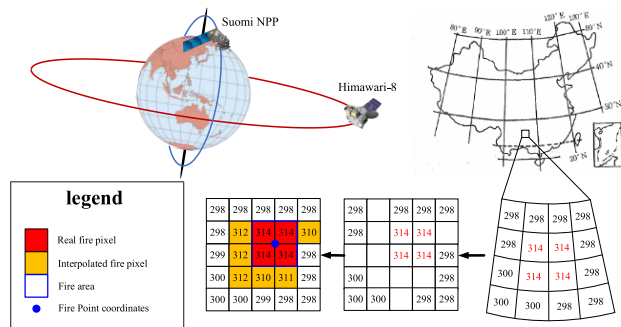


**FIGURE 6.** Fire point latitude and longitude output diagram.

Historical operation experience shows that the fire point beyond 3km from the transmission line will not affect the operation of the transmission line [17]. The entire target area was divided into refined grids ( $0.001^\circ \times 0.001^\circ$ ) as shown in Figure 7. Then extract the line and pole and latitude and longitude information from the grid geographic information

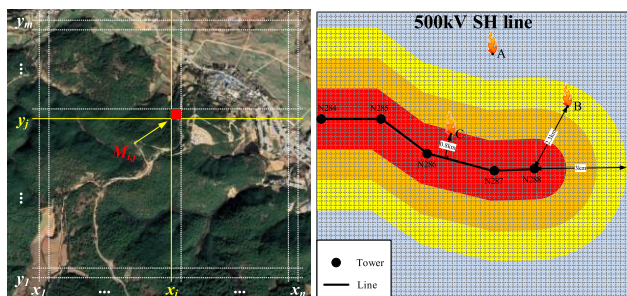


**FIGURE 7.** Grid division of target area and wildfire warning corridor.

system to pre-store in the corresponding grid. The wildfire warning corridor of 3km on each side of the overhead line was drawn, no warning for fire points beyond 3km, and the corridor boundary is smoothed by interpolation.

**III. COMPREHENSIVE FRIE RISK ASSESSMENT BASED ON VARIABLE WEIGHT COEFFICIENT**

First of all, locate the specific grid according to the coordinates of the output fire point and extract the prestored information to determine whether the fire point is within the range of the wildfire warning corridor of the transmission line. Then, calculate each comprehensive element score according to the scores and constant weight coefficients of each sub-element. Finally, the variable weight coefficients of the comprehensive factors are calculated through the constant weight coefficients of the comprehensive factors, and the weighted superposition is used to obtain the comprehensive score.

**A. STANDARDIZATION OF SCORING CRITERIA**

In order to scientifically and accurately assess the risk level of wildfires in transmission line corridor, this paper intends to construct an evaluation system from four aspects: meteorological elements, underlying surface elements, terrain elements and grid elements. Each comprehensive element establishes a scoring criterion with a positive indicator to unify the scoring criteria, that is, the smaller the score, the higher the corresponding wildfire risk rating.

**1) METEOROLOGICAL ELEMENTS**

Temperature, relative humidity and wind speed are the key meteorological elements that affect the spread of wildfires [36]. Calculate temperature, relative humidity and wind speed of fire points corresponding to wildfire alarm of the transmission line issued by Guangdong Power Grid from 2015.01 to 2019.12. In order to evaluate whether the fire points monitored by satellites can develop into wildfires that affect the transmission line tripping, it is necessary to construct meteorological elements evaluation criteria.

**2) UNDERLYING SURFACE ELEMENTS**

In addition to meteorological elements, wildfires also need to have some combustible materials. If there is more combustible material in a certain area, the possibility that the spread of fire point will affect the operation of the transmission line is also greater. Therefore, this paper normalizes the load of combustibles in a positive direction and formulates a scoring rule on a 100-point scale.

$$S_c = 100(1 - c_n/c_{max}) \quad (21)$$

where:  $c_{max}$  is the maximum combustible load in the target area;  $c_n$  is the combustible load near the fire point.

There are many types of vegetation around the transmission line. The energy density, flame intensity and smoke concentration generated by the combustion of different vegetations directly affect the spread speed of wildfires and

TABLE 2. Meteorological elements score table.

Meteorological elements	Scoring formula
Temperature	$S_t = \begin{cases} 100 - \frac{100}{1 + [0.25(38 - t)]^{1.5705}} & t \leq 38 \\ 0 & t > 38 \end{cases}$ <p>Where: <math>t</math> is the real-time temperature (°C); <math>S_t</math> is the temperature score.</p>
Relative humidity	$S_h = \begin{cases} 100 - \frac{100}{1 + [0.11(h - 28)]^{1.6433}} & h \geq 28 \\ 0 & h < 28 \end{cases}$ <p>Where: <math>h</math> is the real-time relative humidity (%); <math>S_h</math> is the relative humidity score.</p>
Wind speed	$S_w = \begin{cases} 100 - \frac{100}{1 + [0.09(56 - w)]^{0.85}} & w \leq 5.6 \\ 0 & w > 5.6 \end{cases}$ <p>Where: <math>w</math> is the real-time wind speed (0.1m/s); <math>S_w</math> is the wind speed score.</p>

TABLE 3. Vegetation type score table.

Vegetation Types	Hazardous situation	Score
Coniferous forest, coniferous and broadleaved mixed forest	Large fire potential and high flame, easy to reduce the insulation strength of the transmission line to the ground and cause the transmission line to trip	25
Broadleaved forest, thickets	Combustion easily forms dense smoke, ionizes under high-temperature and high-pressure conditions, and forms a conductive band, which causes the transmission line to trip	50
Straw crops such as grass, meadows, rice and corn	It is difficult to form a large flame, high temperature and thick smoke, so it is not easy to cause the transmission line to trip	75
Orchards, tea gardens and other low-gross crops	Generally, it will not cause tripping accidents of transmission lines	100

the probability of tripping on transmission lines [37]. The vegetation types in China and their scores are shown in the table below [38].

3) TERRAIN ELEMENTS

Slope has a great effect on the speed gain of fire propagation [39]. Generally, the greater the slope, the faster the speed of wildfire spread, and the corresponding higher risk level. Therefore, this paper adopts formula (22) to normalize the slope and formulate the rule of percentage score.

$$S_s = 100(1 - s_n/s_{max}) \tag{22}$$

where:  $s_{max}$  is the maximum slope of the target area,  $s_n$  is the slope near the fire point.

The aspect of the slope affects the amount of solar radiation received by the ground, which affects the water content of the vegetation and the temperature difference between different aspect. China is located in the northern hemisphere, which results in the southern slope receiving more solar radiation than the northern slope.

TABLE 4. Aspect factor score table.

Aspect	sunny slope	half-sunny slope	half-shady slope	shady slope
Score	25	50	75	100

4) POWER GRID ELEMENTS

The distance between the satellite monitoring fire point and the transmission line directly determines the time when the wildfire spreads below the line. According to the distance between the fire point and the line, the score is obtained by converting it according to formula (23).

$$S_d = 100(d/3) \tag{23}$$

Another element is the importance of the transmission line, which is distinguished according to the voltage level of the line and the functions it undertakes. The critical important line is rated 0, and the noncritical important line is rated 50.

B. CALCULATION METHOD OF THE WEIGHT COEFFICIENT OF EACH ELEMENT

1) ENTROPY METHOD

In this paper, the entropy weight method is used to calculate the constant weight coefficient of each sub-element in each comprehensive element. The entropy method is an objective weighting method, which determines the weight coefficient of each element according to the calculation of the information entropy of each sub-element, which can effectively avoid the influence of human subjective factors. Proceed as follows:

1) Construct sub-element data matrix:

$$S = \begin{bmatrix} s_{11} & \cdots & s_{1n} \\ \vdots & \ddots & \vdots \\ s_{m1} & \cdots & s_{mn} \end{bmatrix} \tag{24}$$

where:  $s_{ij}$  is the score of the  $j$ th element of the  $i$ th wildfire event.

2) Standardization of data:

Various evaluation elements are involved in the construction of the evaluation system, so the dimensions and orders of magnitude of each element will be different, and each element needs to be standardized. However, this article has already carried out the standardization of the percentage system when formulating the scoring rules, and the above element systems are all positive, that is, the smaller the element score, the higher the fire risk rating.

3) Calculate the proportion of the  $j$ th element under the  $i$ th case

$$p_{ij} = s_{ij} / \sum_{i=1}^m s_{ij} \tag{25}$$

Construct the proportion matrix  $P = [p_{ij}]_{m \times n}$ .



4) Calculate the information entropy of each element:

$$e_j = -\frac{1}{\ln m} \sum_{i=1}^m p_{ij} \ln p_{ij} \quad (26)$$

Constructing element information entropy sequence  $E = \{e_1, \dots, e_n\}$ .

5) Calculate the entropy redundancy of each element:

$$d_j = 1 - e_j \quad (27)$$

Constructing the sequence of element entropy redundancy  $D = \{d_1, \dots, d_n\}$ .

6) Calculate the weight coefficient of each element:

$$w_j = d_j / \sum_{j=1}^n d_j \quad (28)$$

Construct a sequence of factor weight coefficients  $W = \{w_1, \dots, w_n\}$ .

This paper uses the data of the historical wildfire trip cases from 2015.1 to 2019.12 to calculate the constant weight coefficients of each sub-element as shown in Table 5. Since there is no distance from the satellite fire point to the line in the historical wildfire trip data, it is impossible to use the entropy weight method to determine the weight coefficient of each sub-element. After consulting with relevant experts, the weight coefficient of the distance and the importance are both set to 0.5.

TABLE 5. Constant weight coefficient of each sub-element.

Comprehensive elements	Sub-elements	Constant weight coefficient
Meteorological elements	Temperature	0.1145
	Relative humidity	0.2920
	Wind speed	0.5934
Underlying surface elements	Combustible load	0.7134
	Vegetation Types	0.2866
Terrain elements	Slope	0.1027
	Aspect	0.8973
Grid elements	Fire point to line distance	0.5000
	Importance of transmission lines	0.5000

## 2) VARIABLE WEIGHT COEFFICIENT

The use of entropy weight method can improve the situation that traditional subjective weighting relies too much on subjective consciousness, but the constant weight coefficient will not change with the change of the comprehensive factor score. When the score of a comprehensive element in the fire risk evaluation element system of the transmission line is very low, the fire point may pose a threat to the operation of the transmission line. If the fire risk level is still calculated based only on the constant weight coefficient, the fire risk level may be low due to the relatively low weight of this element, which is not enough to attract the attention of the staff on duty. Therefore, the constant weight coefficient alone

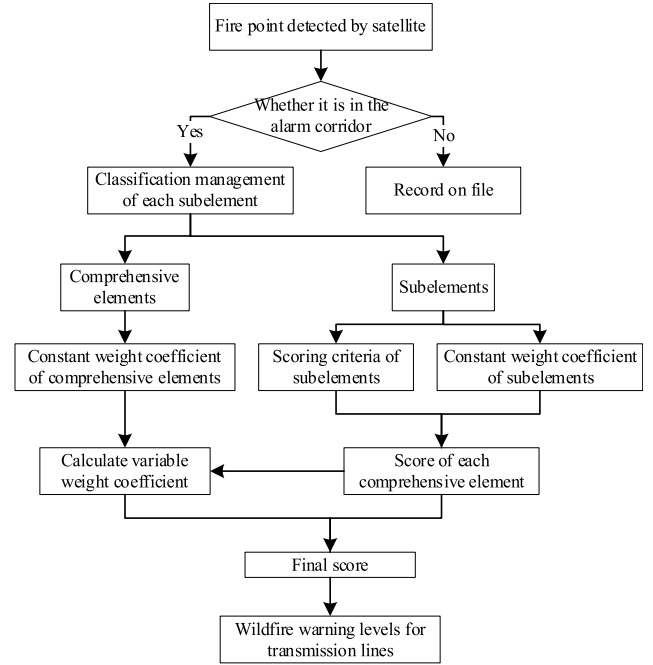


FIGURE 8. Flow chart of comprehensive alarm for fire point in transmission line corridor.

cannot accurately and scientifically reflect the fire risk rating of transmission lines. The variable weight theory in the factor space theory can dynamically adjust the weight of each element in the risk assessment system of transmission lines [40]. The variable weight formula is:

$$w_i^v = w_i s_i^{-1} / \sum_{k=1}^4 w_k s_k^{-1} \quad (29)$$

where:  $w_i^v$  is the variable weight coefficient of the  $i$ th integrated element;  $s_i$  is the comprehensive score value of the  $i$ th integrated element;  $w_i$  is the constant weight coefficient of the  $i$ th integrated element, and the value is 1/4 in this paper.

When the score of a comprehensive element is low, the variable weight formula can automatically adjust the weight coefficient according to its specific score. The lower the score, the greater the variable weight coefficient, which can reflect the real fire risk level. According to the final score, the wildfire risk is divided into five levels as shown in Table 6.

## IV. RESULTS

The wildfire monitoring and warning method based on multi-source satellites for transmission lines is proposed in this paper. It has been applied to the wildfire monitoring system of the transmission line of China Southern Power Grid. From 2019 to 2020, a total of 952 wildfire warnings that may affect the operation of overhead transmission lines of 110kV and above have been issued. The feedback from the on-site inspection line of the operation and maintenance department confirmed that 857 wildfires actually existed, 43 missing alarm fire points, with an accuracy rate of 86.13%. The previous method of using a single geostationary weather satellite to

TABLE 6. Classification of fire risk warning levels based on comprehensive scoring.

Risk level	Score range	Specific description
I	81-100	Will not affect the operation of transmission lines.
II	61-80	Temporarily does not affect the normal operation of the transmission line.
III	41-60	Continue to pay attention to the fire point dynamics.
IV	21-40	If it is far away from the line, continue to pay attention to the dynamics of the fire; If it is close to the line, notify the power supply bureau to carry out on-site inspections.
V	0-20	If it is far away from the line, notify the power supply bureau to carry out on-site inspections. If it is close to the line, consider informing the dispatch center to prepare to shut down the line.

monitor wildfires has an accuracy of less than 70%, and the accuracy of a single polar-orbiting weather satellite is even lower. Figure 9 shows that the highest accuracy rate is Guangdong and the lowest is Guizhou. False alarms and missed alarms mainly occur in Guangxi, Yunnan and Guizhou. There are many reasons for false alarms, while missing alarms are mainly caused by the occlusion of thick clouds and mountains in high altitude areas. In order to verify the comprehensive risk assessment strategy proposed in this paper, the data of real fire points and missing alarm fire points are calculated. Among them, the fault samples (53) are cases where the line is actively stopped or passively tripped, and the normal samples (847) are cases where the wildfire does not affect the operation of the transmission line. According to the final score of samples, the grade distribution is determined as shown in Figure 10. If the traditional distance warning strategy is adopted, the personnel on duty will announce a total of 619 fire spots with a distance of 0~2km from the line, but 3 fault sample (in the blue box) will be missed. With the warning strategy mentioned in this article, the personnel on duty only need to publish a total of 174 fire points (in the red box) that are close to the line and have a higher risk level, which improves the efficiency of operation and maintenance of mountain fire prevention and includes all fault samples. The strategy can provide decision-making basis for the operation and maintenance personnel to carry out the anti-wildfire work during the period of high incidence of wildfire, and greatly reduce the pressure (445/619) of operation and maintenance.

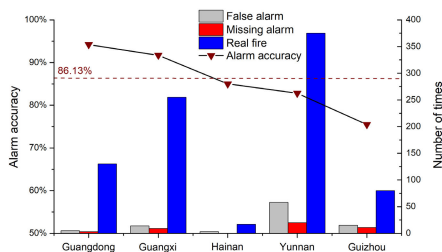


FIGURE 9. Wildfire warnings in 5 provinces under the jurisdiction of China Southern Power Grid.

Based on the advantages of Suomi NPP’s high accuracy, the use of complementary monitoring methods during its transit period can reduce missing alarm rate for small fires. Figure 11 shows the observation image of Guizhou Province at 13:52 on March 8, 2020. The left and right are the infrared

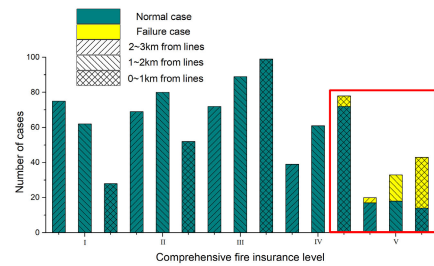


FIGURE 10. According to the distribution of real fire cases, two methods of classification of fire risk alarm levels are verified.

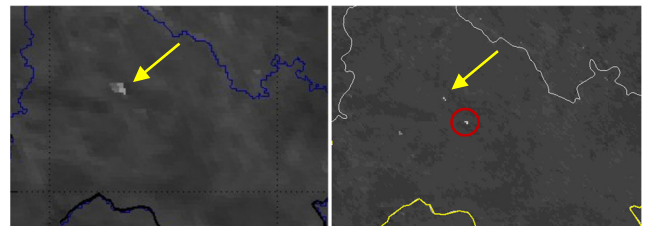


FIGURE 11. Suomi NPP (right) and Himawari-8 (left) sensitivity comparison.

images monitored by Himawari-8 and Suomi NPP respectively. Only one abnormally high temperature point can be found in the left picture, and there are two other hot spots missed by Himawari-8 in addition to the same hot spot pointed by the yellow arrow in the right picture. The hot spot marked by the red circle is exactly within the range of the 500kV JH line alarm corridor. The operation and maintenance personnel inspected the line and found that there is a wildfire that has developed below the line. There are many similar phenomena, which cannot be enumerated due to the limited space.

Based on the high frequency characteristics of Himawari-8, the fire can be detected in time. The system monitored a hot spot affecting transmission lines of 110kV and above at 9:40 on April 2, 2020. The development process is shown in Figure 12, there is no obvious abnormality in the visible light image of the first two times, while the infrared image of 9:30 can see a faint bright spot but has not reached the alarm threshold. The fire point has matured until 9:40, an obvious bright spot appears in both infrared and visible light images. The bright spot is located in the alarm range of the line corridor. The fire point (99.327E, 26.016N) is located in Yunlong County, Dali Bai Autonomous Prefecture, Yunnan

**TABLE 7. Classification of fire risk warning levels based on comprehensive scoring.**

Comprehensive elements	Sub-elements	State value	Sub score	Com score	Constant weight	Variable weight	Final score
Meteorological elements	Temperature	25.4°C	85.8	47.1	0.25	0.09	17.4
	Relative humidity	31%	40.1				
	Wind speed	4.8m/s	43.1				
Underlying surface elements	Combustible load	36.3t/km <sup>2</sup>	1.1	7.9	0.25	0.55	
	Vegetation Types	Coniferous forest	25				
Terrain elements	Slope	16°	52.9	27.9	0.25	0.16	
	Aspect	sunny slope	25				
Grid elements	Fire point to line distance	1.3km	43.3	21.7	0.25	0.2	
	Importance of transmission lines	Yes	0				

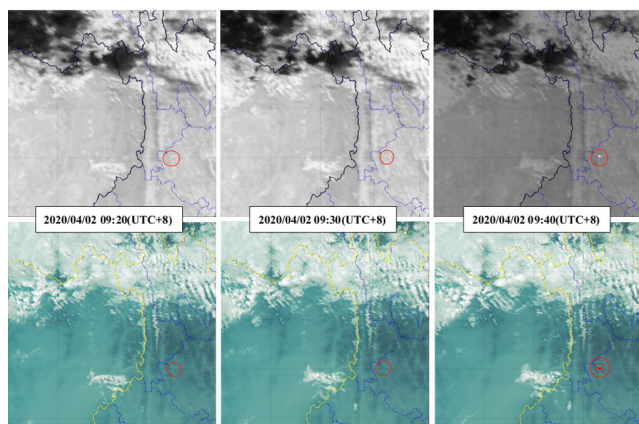


**FIGURE 12. Infrared (upper) and visible (lower) images at different times.**

Province. The section of the affected tower is 500kV MX line (N47-N54). The real-time data collected near the fire point is shown in Table 7. The comprehensive score of the underlying surface element is only 7.9, and the final score belongs to the V-level risk. It is recommended that relevant departments immediately carry out line checking work and report to the dispatch center. According to the feedback from the operation and maintenance personnel on-site line inspection, the alarm fire point is located 150 m to the left of the N51-N54 section of the 500kV MX line. The fire is large and the surrounding vegetation is dense, which can easily cause the transmission line to trip. The dispatch center immediately suspends the transmission line after receiving the message.

**V. DISCUSSION**

In the past, the use of satellite remote sensing technology to monitor wildfires mostly used polar orbiting meteorological satellites based on their high-precision characteristics, but they would only pass through China during a specific period of time, which inevitably caused missing warnings. They are only suitable for large-scale fires in forests and grasslands with low timeliness requirements, and cannot meet the demand for real-time monitoring of wildfires in transmission line corridors. Geostationary meteorological satellites are synchronized with the rotation of the earth and

can perform 24-hour uninterrupted high-frequency observations in a fixed area [41]. However, their spatial resolution is relatively low, resulting in weaker ability to monitor and identify small areas of wildfires such as weeds and shrubs that may cause the transmission line to trip. In this paper, combining the advantages of the two, we use the more advanced Suomi NPP in polar orbiting satellites and the more advanced Himawari-8 in geostationary satellites to perform complementary monitoring of wildfires in the transmission line corridor. At present, the more mature fire point identification algorithms mainly include threshold method, context method and three-band synthesis method [9]–[14]. The brightness temperature changes observed by polar orbiting meteorological satellites are small, and a fixed threshold is usually used for fire point identification, and then appropriate adjustments are made according to the target area [17], [42]. This paper is based on the traditional Suomi NPP relative threshold method to adjust and obtain an improved relative threshold through thermal anomaly analysis. The altitude and observation mode of geostationary meteorological satellites are different from those. Their brightness temperature varies with the observation period and region. Traditional fire point identification algorithms cannot be directly applied to geostationary satellites. Therefore, this paper proposes a fire point identification algorithm based on adaptive dynamic threshold. The actual operation shows that the accuracy of fire spot identification exceeds 85%, which can accurately monitor wildfires in the transmission line corridor.

In view of the cumbersome calculation of fire points associated towers, several fire points location algorithms are proposed: traversal algorithm, circular buffer algorithm, adjacent grid algorithm, area block search algorithm and improved fire points tower location algorithm [5], [17]. Although they have achieved good results, the calculation speed is still not ideal. The fire points location method based on the refined grid prestored geographic information in this paper only judges the grid where the fire point is located, and can determine the tower section affected by the fire point. Compared with other algorithms, the calculation time is reduced by 1 to 4 orders of magnitude, which greatly improves the positioning efficiency. Existing wildfire warning strategies usually determine

the fire risk level according to the distance between the fire point and the line after judging that there is a transmission line corridor around the fire point [5], [17], [43], which cannot meet the accuracy requirements of the transmission line wildfire warning system. Based on the trip risk assessment in the reference [44], this paper comprehensively considers the meteorological elements, underlying surface elements, topographic elements and power grid elements that may affect the spread of wildfires and triggering wildfire tripping of transmission lines, and proposes a comprehensive fire risk assessment strategy based on variable weight coefficients. Practical results show that this strategy can provide scientific basis for operation and maintenance personnel, and can reduce about 70% of the workload during the high-incidence period of wildfires.

This paper uses two satellites to monitor the fire point in a complementary manner, mainly relying on Himawari-8 high-frequency observations every 10 minutes in the actual application process. The disadvantage of this paper is that the use of Suomi NPP to supplement the accuracy of Himawari-8 is very limited, which will cause some small fire points to miss warnings. The limitation of this paper is that the adaptive dynamic threshold can be applied to the whole China, while the improved relative threshold is only applicable to southern China. In the future, we plan to supplement geostationary satellites by fusing multiple polar-orbiting satellites to reduce the missed detection rate of small fire points, and study a universal fire point identification algorithm suitable for polar-orbiting satellites. Wildfires obscured by thin clouds and broken clouds can be effectively identified by the time method, but a feasible method for identifying large areas of thick clouds has not yet been found. As for the situation where wildfires are blocked by mountains in high-altitude areas, we will mark these areas in follow-up research, install fixed mountain fire monitoring devices in important line sections passing through the area, and build a world-ground integrated wildfire warning system.

## VI. CONCLUSION

This paper proposes a complementary monitoring method of wildfires in transmission line corridors based on satellite remote sensing technology. Combined with the high precision of Suomi NPP and the high frequency of Himawari-8, the improved threshold condition and the adaptive dynamic threshold condition are used for fire point identification respectively. Engineering practice shows that the method has high accuracy and reduces the misjudgment and missed judgment of fire point to a certain extent. A comprehensive warning strategy is proposed for the detected fire point, which is analyzed from the four aspects of meteorological elements, underlying surface elements, terrain elements and power grid elements that affect the spread of wildfires and cause transmission line trips. Entropy weight method combined with variable weight theory is used to dynamically adjust the weight of each comprehensive element, according to the final score of weighted superposition to determine alarm level.

The strategy can objectively and scientifically assess the risk level of wildfires in transmission line corridors, It provides decision-making basis for emergency treatment of wildfire disasters, greatly reduce the pressure of transmission and maintenance of transmission personnel.

## REFERENCES

- [1] T. Wu, J. J. Ruan, Y. Hu, B. Liu, and C. Chen, "Research on the characteristics and mechanism of mountain fire breakdown of 500 kV transmission lines," *Chin. Soc. Electron. Eng.*, vol. 31, no. 34, pp. 163–170, 2011.
- [2] Y. J. Wu, Y. S. Xue, J. Z. Lu, Y. Y. Xie, T. S. Xu, W. Y. Li, and C. Wu, "Spatiotemporal impact of mountain fire disaster on power grid failure rate," *Autom. Electron. Power Syst.*, vol. 40, no. 3, pp. 14–20, 2016.
- [3] Y. Zeng, "Research on the risk assessment method of forest transmission band based on the temporal and spatial characteristics of mountain fire," M.S. thesis, Dept. Electron. Eng., Chongqing Univ., Chongqing, China, 2017.
- [4] J. Z. Lu, T. J. Zhou, C. P. Wu, B. Li, Y. J. Tan, and Y. Zhu, "Statistics and analysis of 220 kV and above transmission line faults in a provincial power grid," *High Voltage Technol.*, vol. 42, no. 1, pp. 200–207, 2016.
- [5] Y. Liu, J. Z. Lu, J. Luo, G. Y. Zhang, and L. F. He, "Mountain fire synchronous satellite wide area monitoring and pole tower positioning of overhead transmission lines," *Power Syst. Technol.*, vol. 42, no. 4, pp. 1322–1327, 2018.
- [6] X. Y. Chen, T. Yang, C. R. Yin, X. B. Shen, C. Z. Xie, D. Dai, and M. Zhang, "Method for monitoring fire on transmission line based on LiDAR technology," *Laser Infr.*, vol. 44, no. 11, pp. 1202–1206, 2014.
- [7] K. H. Huang, D. Y. Zhang, J. He, and Y. P. Huang, "The application of a new generation of Doppler weather radar in forest fire monitoring. Forest," *Sci. Technol.*, vol. 32, no. 5, pp. 33–36, 2007.
- [8] L. P. Ye, X. Y. Chen, Z. L. He, C. Z. Xie, J. H. Huang, Y. F. Xia, and D. Dai, "Application status of hill fire warning technology in transmission lines," *Power Syst. Protection Control*, vol. 42, no. 6, pp. 145–153, 2014.
- [9] X. Xiao, "Research on MODIS forest fire monitoring method based on inter-class variance," M.S. thesis, Dept. Electron. Eng., Univ. Sci. Technol. Chin., Hefei, China, 2019.
- [10] C. O. Justice, J. D. Kendall, P. R. Dowty, and R. J. Scholes, "Satellite remote sensing of fires during the SAFARI campaign using NOAA-AVHRR data," *J. Geophys. Res.*, vol. 101, no. D19, pp. 23851–23863, 1996.
- [11] Y. X. Xing, D. F. Nan, L. Yu, and S. Q. Zhou, "Research and development of forest fire warning system," *Comput. Knowl. Technol.*, vol. 7, no. 16, pp. 3923–3927, 2011.
- [12] L. Giglio, J. Desclotres, C. O. Justice, and Y. J. Kaufman, "An enhanced contextual fire detection algorithm for MODIS," *Remote Sens. Environ.*, vol. 87, nos. 2–3, pp. 273–282, Oct. 2003.
- [13] S. P. Flasse and P. A. Ceccato, "Contextual algorithm for AVHRR fire detection," *Int. J. Remote. Sens.*, vol. 17, no. 2, pp. 419–424, 1996.
- [14] Z. X. Xie, "Fire point detection and automatic cloud detection based on Himawari-8 remote sensing data," M.S. thesis, Dept. Electron. Eng., Univ. Sci. Technol. Chin., Hefei, China, 2019.
- [15] J. Z. Lu, C. P. Wu, L. Yang, H. X. Zhang, Y. Liu, and X. J. Xu, "Research and application of mountain fire monitoring and early warning system for transmission lines," *Power Syst. Prot. Control.*, vol. 42, no. 16, pp. 89–95, 2014.
- [16] Q. Y. Jiang and M. Y. Yan, "Probability statistics-based fire monitoring method for transmission lines," *High Voltage Technol.*, vol. 41, no. 7, pp. 2302–2307, 2015.
- [17] J. Z. Lu, Y. Liu, C. P. Wu, H. X. Zhang, and T. J. Zhou, "Research on mountain fire satellite monitoring and warning algorithms for transmission lines," *Chin. Soc. Electron. Eng.*, vol. 35, no. 21, pp. 5511–5519, 2015.
- [18] J. Chen, W. Zheng, and C. Liu, "Himawari-8 static weather satellite grassland fire monitoring and analysis," *J. Natural Disaster*, vol. 26, no. 4, pp. 197–204, 2017.
- [19] X. W. Li, Z. C. Niu, S. Jiang, and H. Shi, "Environmental monitoring satellite Suomi NPP business characteristics and ecological environment monitoring application," *Environ. Monit. Forewarning*, vol. 6, no. 3, pp. 1–6, 2014.
- [20] X. Jing, X. Q. Hu, S. Y. Zhao, L. Q. He, X. B. Hu, and L. Yan, "VIIRS mid-infrared sea surface flare zone reflectance calculation based on improved nonlinear window splitting algorithm," *Spectrosc. Spect. Anal.*, vol. 37, no. 2, pp. 394–402, 2017.

- [21] L. Xia, K. B. Mao, Z. W. Sun, and Y. Ma, "Introduction of Suomi NPP VIIRS data and its application analysis in cloud detection," *Frontiers Earth. Sci.*, vol. 3, no. 5, pp. 271–276, 2013.
- [22] Y. L. Chi, L. Sun, and J. Wei, "Suomi NPP satellite visible infrared imaging radiometer improved dynamic threshold cloud detection algorithm," *Acta Optica Sinica*, vol. 39, no. 5, pp. 360–370, 2019.
- [23] X. Jing, L. Yan, X. Q. Hu, L. Q. He, S. Y. Zhao, X. B. Hu, H. L. Xu, Y. Lin, and A. N. Ma, "Verification of on-orbit NPP/VIIRS reflection band based on sea surface flare mid-infrared reference," *J. Infr. Millim. Wave.*, vol. 36, no. 6, pp. 694–700, 2017.
- [24] K. Bessho et al., "An introduction to Himawari-8/9—Japa's new-generation geostationary meteorological satellites. J. Meteorologic," *Soc. Japan.*, vol. 94, pp. 151–183, 2016.
- [25] *Himawari Standard Data User's Guide [EB/OL]*, Japan Meteorological Agency, Tokyo, Japan, 2013.
- [26] P. Zhang, Q. Guo, B. Y. Chen, and X. Feng, "Comparative analysis of the Fengyun 4 meteorological satellite in my country and the Himawari-8/9 satellite in Japan," *Meteorological Sci. Technol. Prog.*, vol. 6, no. 1, pp. 72–75, 2016.
- [27] J. Chen, A. Liao, J. Chen, S. Peng, L. J. Chen, and H. W. Zhang, "30-meter GlobalLand cover data product GlobeLand30," *Geomatic. World*, vol. 24, no. 1, pp. 1–8, 2017.
- [28] H. T. Guo, Y. Wang, X. P. Liu, and Z. H. Jiang, "A comprehensive optimization method for satellite cloud image cloud detection," *J. PLA Univ. Sci. Technol.*, vol. 11, no. 2, pp. 221–227, 2010.
- [29] Y. Kaufman, C. Ichoku, L. Giglio, S. Korontzi, D. Chu, W. Hao, R. Li, and C. Justice, "Fire and smoke observed from the earth observing system MODIS instrument products, validation, and operational use," *Int. J. Remote Sens.*, vol. 24, no. 8, pp. 1765–1781, 2003.
- [30] X. C. Zhou and X. Q. Wang, "EOS-MODIS data forest fire recognition algorithm verification and improvement," *Remote Sens. Technol. Appl.*, vol. 21, no. 3, pp. 206–211, 2006.
- [31] E. Z. Zhou, Y. Huang, J. Chen, R. Z. Wei, T. Wang, and S. Y. Sui, "Mountain fire identification method in Guangdong and its application in power grid," *Meteorological Sci. Technol.*, vol. 48, no. 1, pp. 132–140, 2020.
- [32] N. Shan, T. Y. Zheng, and Z. S. Wang, "Fast and high accuracy cloud detection algorithm and its application," *J. Remote. Sens.*, vol. 13, no. 6, pp. 1138–1155, 2009.
- [33] J. Zhang, W. Y. Zhang, J. D. Feng, H. Y. Wang, Z. Yu, and W. Song, "MODIS fire point monitoring algorithm based on brightness temperature-vegetation index-aerosol optical depth," *Remote. Sens. Technol. Appl.*, vol. 31, no. 5, pp. 886–892, 2016.
- [34] Y. Zhou, S. X. Wang, L. T. Wang, S. R. Chen, and H. C. Li, "Fire point information automatic extraction method based on MODIS data," *J. Natural Disaster*, vol. 16, no. 1, pp. 88–93, 2007.
- [35] X. Xu, J. S. Li, and L. L. Zhao, "Monitoring method of fire point of straw burning based on VIIRS image," *Geospatial Inf.*, vol. 16, no. 6, pp. 90–93, 2018.
- [36] A. Ganteaume, A. Camia, M. Jappiot, J. San-Miguel-Ayanz, M. Long-Fournel, and C. Lampin, "A review of the main driving factors of forest fire ignition over Europe," *Environ. Manage.*, vol. 51, no. 3, pp. 651–662, Mar. 2013.
- [37] J. Z. Lu, T. Zhou, C. Wu, and B. Li, "Differentiation technology and strategy of wildfire protection for transmission lines," *High Voltage Technol.*, vol. 43, no. 8, pp. 2524–2532, 2017.
- [38] *Q/GDW 11643–2016 Drawing Guidelines for Region Distribution Map of Wildfires Near Overhead Transmission Lines*, Hunan China, State Grid Corporation of China, Beijing, China, 2007.
- [39] X. M. Mao, "The influence of wind and relief on the speed of the forest fire spreading," *Quart. J. Appl. Meteorol.*, vol. 4, no. 1, pp. 100–104, 1993.
- [40] W. Q. Liu, "Balanced function and its application for variable weight synthesizing," *Syst. Eng. Theory Pract.*, vol. 17, no. 4, pp. 58–64, 1997.
- [41] L. Na, J. Zhang, Y. Bao, Y. Bao, R. Na, S. Tong, and A. Si, "Himawari-8 satellite based dynamic monitoring of grassland fire in China-Mongolia border regions," *Sensors*, vol. 18, no. 1, p. 276, Jan. 2018.
- [42] L. Giglio, W. Schroeder, and C. O. Justice, "The collection 6 MODIS active fire detection algorithm and fire products," *Remote Sens. Environ.*, vol. 178, pp. 31–41, Jun. 2016.
- [43] J. Z. Lu, C. Wu, Li Yang, H. Zhang, Y. Liu, and X. J. Xu, "Research and application of forest fire monitor and early-warning system for transmission line," *Power Syst. Protection Control.*, vol. 42, no. 16, pp. 89–95, 2016.

- [44] S. Shi, C. Yao, S. Wang, and W. Han, "A model design for risk assessment of line tripping caused by wildfires," *Sensors*, vol. 18, no. 6, p. 1941, Jun. 2018.



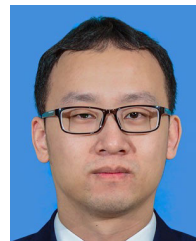
**YU LIANG** received the B.S. degree in electrical engineering from the Shaanxi University of Science and Technology, Xi'an, China, in 2017. He is currently pursuing the M.S. degree in electrical engineering with the Changsha University of Science and Technology, Changsha, China. His research interests include environmental monitoring and disaster early warning near power transmission lines.



**LAWU ZHOU** received the M.S. and Ph.D. degrees in electrical engineering from Hunan University, Changsha, China. He is currently a Professor with the Changsha University of Science and Technology, Changsha. He has authored or coauthored 12 of scientific articles and books. His research interests include energy generation technology, motors and their systems, and grid disaster prevention and mitigation.



**JIE CHEN** received the M.S. degree in meteorological remote sensing from the Chinese Academy of Meteorological Sciences, Beijing, China. He is currently a Senior Engineer with the National Satellite Meteorological Center, Beijing. His research interests include satellite remote sensing ecological environment monitoring and assessment application.



**YONG HUANG** received the M.S. degree in high-voltage engineering from Wuhan University, Wuhan, China. He is currently a Senior Engineer with Electric Power Research Institute of Guangdong Power Grid Company Ltd., Guangzhou, China. His research interests include power grid disaster prevention and mitigation technology, transmission line fault diagnosis, and power grid disaster loss assessment.



**RUIZENG WEI** received the M.S. degree in meteorological science from Nanjing University, Nanjing, China. He is currently a Senior Engineer with Electric Power Research Institute of Guangdong Power Grid Company Ltd., Guangzhou, China. His research interests include environmental monitoring and weather warning near transmission lines, disaster prevention, and mitigation of power grid.



**ENZE ZHOU** received the M.S. degree in electrical engineering from North China Electric Power University, Beijing, China. He is currently a Senior Engineer with Electric Power Research Institute of Guangdong Power Grid Company Ltd., Guangzhou, China. His research interests include transmission line fault diagnosis and wildfires monitoring near the transmission line corridor.